Journal of Molecular Structure 1053 (2013) 89–99

Contents lists available at ScienceDirect

Journal of Molecular Structure

journal homepage: www.elsevier.com/locate/molstruc

Synthesis, characterization and antimicrobial studies of 2-{(*E*)-[(2-hydroxy-5-methylphenyl)imino]methyl}-4-[(*E*)-phenyldiazenyl] phenol as a novel azo-azomethine dye

Muhammet Köse [a], Nurcan Kurtoglu [b], Özkan Gümüşsu [b], Mustafa Tutak [c], Vickie McKee [d], Duran Karakaş [e], Mukerrem Kurtoglu [a,*]

[a] Department of Chemistry, Kahramanmaras Sutcu Imam University, Kahramanmaras 46050, Turkey
[b] Department of Textile, Kahramanmaras Sutcu Imam University, Kahramanmaras 46050, Turkey
[c] Department of Textile, Erciyes University, Kayseri 38000, Turkey
[d] Department of Chemistry, Loughborough University, Leics. LE11 3TU, UK
[e] Department of Chemistry, Faculty of Science, Cumhuriyet University, 58140 Sivas, Turkey

HIGHLIGHTS

- A novel azo-azomethine dye was synthesized and characterized by elemental analysis, FT-IR, ^{1}H, ^{13}C NMR and mass spectroscopy.
- Molecular structure of the dye was determined by single crystal X-ray diffraction study.
- The effect of various organic solvents with different polarities on the UV–Vis. spectra of the dye has been studied.
- Furthermore, the pathogenic activities of the synthesized dye was tested *in vitro* against the sensitive organisms, *Bacillus cereous* and *Staphylococcus aureus, Escherichia coli*, and *Klebsiella pneumoniae*.

GRAPHICAL ABSTRACT

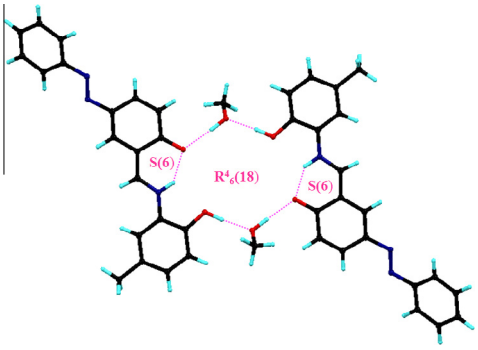

ARTICLE INFO

Article history:
Received 26 July 2013
Received in revised form 26 August 2013
Accepted 10 September 2013
Available online 14 September 2013

Keywords:
Synthesis
Azo-azomethine
X-ray structure
Tautomerism
Solvent effect
Biological activity

ABSTRACT

A novel dye, 2-{(*E*)-[(2-hydroxy-5-methylphenyl)imino]methyl}-4-[(*E*)-phenyldiazenyl]phenol dye was synthesized by the condensation reaction of 2-hydroxy-5-[(*E*)-phenyldiazenyl]benzaldehyde with 2-amino-4-methylphenol in methanol. The title dye was characterized by its melting point, elemental analysis, FT-IR, ^{1}H, ^{13}C NMR and mass spectroscopic studies. Molecular structure of the title dye was determined by single crystal X-ray diffraction study. X-ray data showed that the dye crystallizes in the monoclinic space group $P2_1/c$ with cell parameters $a = 18.541(2)$ Å, $b = 4.7091(5)$ Å, $c = 20.586(2)$ Å, $V = 1761.5(3)$ Å^3 and $Z = 4$. The title dye adopts azo-enamine tautomer in the solid state. The molecules crystallises as dimers assembled by two molecules of methanol *via* intermolecular hydrogen bonding resulting in $R_6^4(18)$ hydrogen bonding motif. Additionally, there is an intramolecular keto-amine hydrogen bond (NH···O) with a distance of 2.6172(17) Å. Optimized structures of the three possible tautomers of the compound were obtained using B3LYP method with 6-311++G(d,p), 6-31G and 3-21G basis sets in the gas phase. Thermal properties of the prepared dye were examined by thermogravimetric analysis and results indicated that the framework of the dye is stable up to 172 °C. Furthermore, the pathogenic activities of the synthesized dye were tested *in vitro* against the sensitive organisms, *Bacillus cereous* (ATCC 33019) and *Staphylococcus aureus* (ATCC 25923) as gram positive bacteria, *Escherichia coli*

* Corresponding author. Tel.: +90 344 280 1450; fax: +90 344 280 1352.
E-mail addresses: kurtoglu01@gmail.com, mkurtoglu@ksu.edu.tr (M. Kurtoglu).

0022-2860/$ - see front matter
http://dx.doi.org/10.1016/j.molstruc.2013.09.013

(ATCC 11229), and *Klebsiella pneumoniae* (ATCC 13883) as gram negative bacteria and the results are discussed. The results indicated that the prepared dye had antibacterial activities against gram-positive bacteria (*S. aureus* and *Bacillus cereuss*), but it exhibited no activity against gram-negative bacteria (*E. coli* and *K. pneumoniae*).

1. Introduction

Compounds containing azo groups are of great interest because of a wide range of applications such as organic dyes [1], indicators [2], radical reaction initiators [3] and therapeutic agents [4]. Azo dyes are in use as dyestuffs for wool, leather and synthetic fabrics due to their excellent coloring properties [5]. Compounds containing both imine (—C=N—) and azo (—N=N—) groups are also important structures in medicinal and pharmaceutical chemistry and it has been suggested that the azomethine linkage might be responsible for the biological activities displayed by Schiff bases [6,7]. These compounds have also received special attention in coordination chemistry due to their mixed hard–soft donor character and versatile coordination behavior [8–11].

Recently, the study of azo-azomethine dyes containing hydroxyl groups has attracted considerable attention [12–17]. Inter- and intramolecular proton transfer from phenolic oxygen to imine nitrogen is very common in polyhydroxy derivatives of azo-azomethine dyes resulting in a self-isomerisation [13]. Due to proton transfer ability of azo-azomethine dyes, these systems have been of a special interest from practical viewpoint as the tautomers showing different optical behavior and dyeing properties [14]. Determination of which tautomeric structure favoured under certain conditions is important in terms of coloristic and technological properties of dyes. The presence of enol/imine, keto/amine and hydrazone/azo-enaminone tautomerism in azo-azomethine dyes affect their photo-physical and photo-chemical properties [15,16]. Self-isomerisation *via* proton transfer depends on several factors such as temperature, the substituent structure and solvent polarity. Dye–solvent interactions play an important role in tautomerism in solution [16,17]. 5-Arylazo-*o*-hydroxylimines have been reported to show thermochromism and photochromism in the solid state by a proton transfer from the hydroxyl O-atom to the imine N-atom [17].

Recently, some compounds containing both imine and/or azo groups have been reported by our group [18–21]. In this study, we reported the synthesis, crystallographic and spectroscopic studies as well as thermal investigation of a novel salicylaldimine-based compound, 2-{(*E*)-[(2-hydroxy-5-methylphenyl) imino]methyl}-4-[(*E*)-phenyldiazenyl]phenol dye (Scheme 1). ^{13}C and ^{1}H NMR spectra, UV–Vis spectroscopy, mass spectroscopy and elemental analysis were obtained to determine the structure of the azo-azomethine dye. The computational studies of the compound were examined by Gauss View 5.0.8. Thermal properties of the prepared compound were examined by thermogravimetric analysis. The results indicated that the framework of the azo-enamine dye is stable up to 172 °C. Additionally, antimicrobial activity of the title compound was studied using both gram positive and negative bacteria.

2. Experimental

All reagents and solvents for synthesis and analysis were purchased from commercial sources and used as received unless otherwise noted. 2-Hydroxy-5-[(*E*)-phenyldiazenyl]benzaldehyde was prepared according to the published paper [22]. IR spectrum was performed on a Perkin Elmer Paragon 1000PC. CHN analysis was performed using a CE-440 Elemental analyzer. NMR spectra were performed using a Bruker Avance 400. Mass spectrum was recorded on a Thermo Fisher Exactive + Triversa

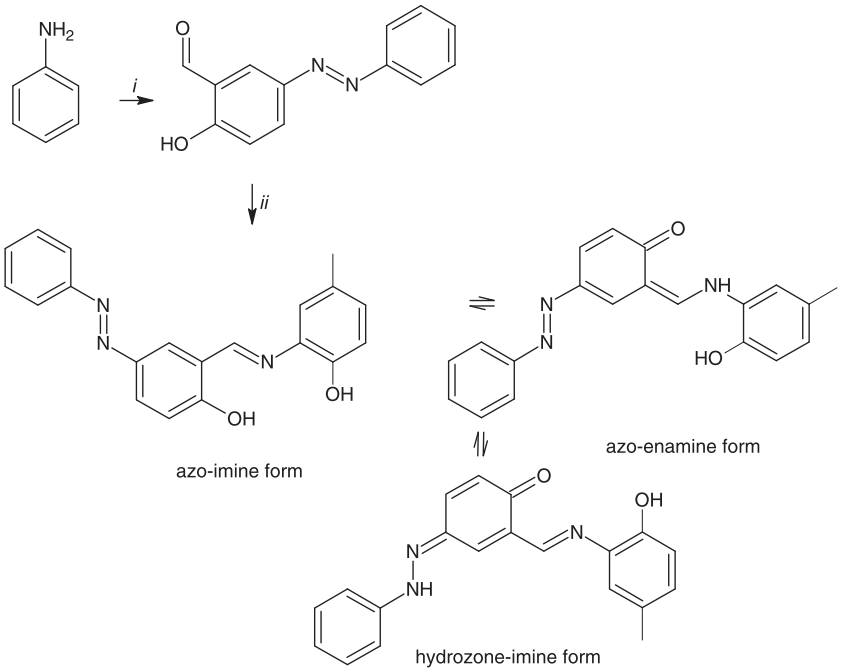

Scheme 1. Synthesis of 2-{(*E*)-[(2-hydroxy-5-methylphenyl)imino]methyl}-4-[(*E*)-phenyldiazenyl]phenol dye and its tautomers. (i) (**1**) $NaNO_2$, HCl, 0 °C, (**2**) salicylaldehyde; (ii) 2-amino-4-methylphenol, MeOH and reflux.

Nanomate mass spectrometer. The UV–Vis spectra were measured with a T80+ UV–Vis. Spectrometer PG Instruments LTD spectrometer. Data collection for X-ray crystallography was completed using a Bruker APEX2 CCD diffractometer and data reduction was performed using Bruker SAINT. SHELXTL was used to solve and refine the structures [23].

2.1. Synthesis, elemental and spectral analysis of 2-{(E)-[(2-hydroxy-5-methylphenyl)imino]methyl}-4-[(E)-phenyldiazenyl]phenol dye

A solution of 2-hydroxy-5-[(*E*)-phenyldiazenyl]benzaldehyde (0.25 g, 1.1 mmol) in methanol (30 mL) was added dropwise to a methanolic solution (20 mL) of 2-amino-4-methylphenol (0.14 g, 1.1 mmol). The reaction mixture was refluxed for two hours, on cooling to room temperature red precipitate formed was collected by filtration. Single crystal suitable for X-ray diffraction studies were grown from the methanol solution of the dye by slow evaporation.

Yield: 0.34 g 86%, color: red. M.p.: 178–179 °C. Anal. Calc. for $C_{20}H_{17}N_3O_2{\cdot}CH_3OH$: C, 69.41; H, 5.82; N, 11.56%. Found: C, 69.24; H, 5.67; N, 11.64%. ESI-MS (*m*/*z* (rel. intensity) assignment): 332 (26%) $[M+H]^+$, 354 (100%) $[M+Na]^+$, 685 $[M_2+Na]^+$ (8%). ^1H NMR: (d-DMSO as solvent, δ in ppm,): 15.07 (*s*, 1H, —N1—H), 9.87 (*s*, 1H, O1—H), 9.25 (*s*, 1H, C8—H), 6.22–8.27 (11H, aromatic), 4.17 (s, 1H, —O3—H), 3.22 (s, 3H, C21—H_3), 2.16 (s, 3H, C5—H_3). ^{13}C NMR (d-DMSO as solvent, δ in ppm): 167.33 (C8), 114.23–159.85 (C, aromatic), 48.57 (C21), 20.48 (C5). IR (cm^{-1}): 3370 (O—H str.); 3190 (N—H str); 3060 (C—H str of aromatic); 2912 (C—H str of aliphatic); 1614 (C10═O2 and C7—N1 str); 1588 (—C═C— str of aromatic); 1480 (—N═N— str); 1207 (C—O str); 1141 and 877 (aromatic C—H bond).

2.2. Theoretical calculations

The structure of azo-enamine **(1)**, azo-imine **(2)** and hydrozone-imine **(3)** forms were prepared with GaussView 5.0.8 [24]. Calculations were made with Gaussian 09 AM64L-Revision-C.01 [25]. Density functional theory (DFT/B3LYP) method which is based on Kohn–Sham theory was used for structure optimizations [26–30]. Tautomer **(1)** was fully optimized with 6-311G(d,p), 6-31+G(d,p) and 3-21G basis sets in gas phase. The best level was found to be B3LYP/6-311G(d,p). After that tautomers **(2)** and **(3)** were fully optimized by using the best level in gas phase. The transition state (TS) method was used to find the transition states [31].

Table 1
Crystallographic data for the dye.

Identification code	Dye
Empirical formula	$C_{21}H_{21}N_3O_3$
Formula weight	363.41
Crystal size (mm^3)	0.33 × 0.25 × 0.08
Crystal color	Red
Crystal system	Monoclinic
Space group	$P2_1/c$
Unit cell	
a (Å)	18.541(2)
b (Å)	4.7091(5)
c (Å)	20.586(2)
α (°)	90
β (°)	101.460(2)
γ (°)	90
Volume (Å3)	1761.5(3)
Z	4
Abs. coeff. (mm^{-1})	0.093
Refl. collected	16609
Completeness to θ = 28.02°	99.6%
Ind. Refl. [R_{int}]	4253[0.0450]
*R*1, *wR*2 [$I > 2\sigma(I)$]	0.0427, 0.0945
*R*1, *wR*2 (all data)	0.0701, 0.1083
CCDC number	950594

Table 2
Hydrogen bond parameters for the dye [Å and °].

D—H···A	d(D—H)	d(H···A)	d(D···A)	<(DHA)
N(1)—H(1A)···O(2)	0.921(18)	1.842(18)	2.6172(17)	140.4(15)
O(3)—H(3A)···O(2)	0.91(2)	1.80(2)	2.7108(16)	176.3(19)
O(1)—H(1)···O(3A)	0.94(2)	1.67(2)	2.6095(16)	175.0(19)

Symmetry operations for equivalent atoms A: −*x*, −*y*, −*z*.

2.3. X-ray crystallography

A single crystal of dimensions 0.33 × 0.25 × 0.08 mm^3 was chosen for the diffraction experiment. Data were collected at 150(2) K on a Bruker ApexII CCD diffractometer using Mo Kα radiation (λ = 0.71073 Å). The structure was solved by direct methods and refined on F^2 using all the reflections [32]. All the non-hydrogen atoms were refined using anisotropic atomic displacement parameters and hydrogen atoms bonded to carbon atoms were inserted at calculated positions using a riding model. Hydrogen atoms bonded to oxygen and nitrogen atoms were located from difference maps and refined with temperature factors riding on the carrier atom. Details of the crystal data and refinement are given Table 1. Hydrogen bond parameters are given in Table 2 and bond lengths and angles are given in Tables 3 and 4, respectively.

2.4. Thermal analyses

Thermal analysis of the dye was performed on SII Exstar TG/DTA 6200. Thermal stability of the dye (~1 mg) was studied in the temperature range of 30–1000 °C under nitrogen atmosphere at a heating rate of 20 °C/min.

2.5. Antimicrobial tests

Cultures of the following four different bacteria were used in the study: before the antimicrobial tests, all bacteria from the fresh culture were grown in nutrient broth at 37 °C for 18 h. Each bacterium culture had 10^7 cfu (colony forming unit)/mL cells.

Diffusion agar test method was used for the dye in dimethyl sulfoxide and sterilized azo-azomethine solutions of four different concentrations (1%, 2%, 3% and 4%) levels. A nutrient agar medium (g/L: peptone 5.0; beef extract 1.5; yeast extract 1.5; NaCl 5.0; agar 20; pH 7.5) was prepared and autoclaved at 121 °C for 15 min. Test organisms were grown overnight at 37 °C, in 10 mL nutrient broth. 1 mL bacterial cultures were added to the cooled 100 mL nutrient agar (1%). Sterilized Petri plates with three wells opened (4 mm in diameter) were prepared with an equal thickness of nutrient agar. 60 μL of the dye solution was poured into wells on nutrient agar. *Escherichia coli*, *Klebsiella pneumoniae*, *Bacillus cereous*, and *Staphylococcus aureus aureus* test Petri plates were incubated at 37 °C for 24 h. At the end of this period, zone of inhibition formed on the medium were measured in millimeters (mm).

3. Results and discussion

3.1. Basic properties of 2-{(E)-[(2-hydroxy-5-methylphenyl)imino]methyl}-4-[(E)-phenyldiazenyl]phenol dye

The red product is stable at room temperature in the solid state without decomposition. The air-stable red product of the azo-azomethine dye is soluble in DMSO, DMF, methanol, ethanol, acetonitrile, and chloroform, and insoluble in hexane and water. Elemental

Table 3
Calculated and experimental bond lengths (Å) of tautomers.

	Tautomer **(1)**				Tautomer **(2)**	Tautomer **(3)**
	Expt.	6-311G(d,p)	6-31+G(d,p)	3-21G	6-311G(d,p)	6-311G(d,p)
O1—C1	1.3528(19)	1.366	1.366	1.382	1.363	1.362
C1—C7	1.398(2)	1.409	1.409	1.412	1.41	1.413
C3—C4	1.398(2)	1.403	1.403	1.399	1.386	1.394
C4—C5	1.511(2)	1.512	1.512	1.519	1.511	1.511
C7—N1	1.4120(19)	1.406	1.406	1.406	1.402	1.398
C8—C9	1.408(2)	1.405	1.405	1.404	1.452	1.466
C9—C10	1.446(2)	1.475	1.475	1.473	1.429	1.503
C10—C11	1.432(2)	1.446	1.446	1.445	1.403	1.473
C12—C13	1.425(2)	1.434	1.434	1.433	1.406	1.448
C13—N2	1.4148(18)	1.407	1.407	1.411	1.41	1.318
N3—C15	1.4268(19)	1.418	1.418	1.426	1.418	1.403
C15—C16	1.395(2)	1.403	1.403	1.401	1.389	1.4
C17—C18	1.385(2)	1.397	1.397	1.397	1.383	1.393
C19—C20	1.386(2)	1.392	1.392	1.39	1.377	1.39
C1—C2	1.391(2)	1.395	1.395	1.39	1.382	1.391
C2—C3	1.386(2)	1.395	1.395	1.396	1.393	1.395
C4—C6	1.389(2)	1.398	1.398	1.4	1.396	1.399
C6—C7	1.392(2)	1.402	1.402	1.396	1.389	1.4
N1—C8	1.3077(19)	1.329	1.329	1.33	1.286	1.274
C9—C14	1.410(2)	1.417	1.417	1.41	1.386	1.363
C10—O2	1.2811(17)	1.262	1.262	1.281	1.332	1.219
C11—C12	1.357(2)	1.367	1.367	1.363	1.372	1.346
C13—C14	1.372(2)	1.384	1.384	1.381	1.385	1.442
N2—N3	1.2617(17)	1.263	1.263	1.298	1.256	1.315
C15—C20	1.389(2)	1.408	1.408	1.404	1.403	1.399
C16—C17	1.381(2)	1.396	1.396	1.393	1.381	1.39
C18—C19	1.380(2)	1.402	1.402	1.401	1.388	1.395

Table 4
Calculated and experimental bond angles (°) of tautomers.

	Tautomer **(1)**				Tautomer **(2)**	Tautomer **(3)**
	Expt.	6-311G(d,p)	6-31+G(d,p)	3-21G	6-311G(d,p)	6-311G(d,p)
O1—C1—C2	124.95(14)	123.9	123.8	125.1	123.0	123.0
C2—C1—C7	118.91(14)	119.5	119.7	119.5	119.5	119.4
C2—C3—C4	121.49(15)	121.0	121.0	120.7	121.1	121.0
C6—C4—C5	121.42(14)	118.2	118.2	118.5	117.8	117.8
C4—C6—C7	121.09(14)	121.7	121.7	121.4	122.3	122.4
C6—C7—N1	123.87(13)	123.7	123.7	124.6	123.8	122.9
C8—N1—C7	127.45(13)	127.4	127.4	127.7	122.4	119.7
C8—C9—C14	119.34(14)	119.3	119.3	120.2	119.8	117.5
C14—C9—C10	119.95(14)	120.8	120.7	121.0	119.3	119.8
O2—C10—C9	121.60(14)	121.8	121.4	121.9	122.0	123.1
C12—C11—C10	122.23(14)	121.4	121.2	121.7	120.3	122.7
C14—C13—N2	117.26(13)	125.3	125.4	125.2	125.0	126.7
N2—C13—C12	124.01(13)	115.8	115.6	116.0	116.2	115.7
N3—N2—C13	113.95(12)	115.9	116.0	115.0	115.5	121.4
C20—C15—C16	119.56(14)	119.5	119.7	119.4	119.7	120.1
C16—C15—N3	124.91(13)	115.7	115.6	116.0	115.6	118.2
C16—C17—C18	120.68(15)	119.9	120.0	119.9	119.9	120.4
C18—C19—C20	119.86(15)	120.5	120.6	120.3	120.5	121.0
O1—C1—C7	116.14(14)	116.6	116.6	115.4	117.5	117.6
C3—C2—C1	120.20(15)	120.5	120.4	120.6	120.6	120.8
C6—C4—C3	117.96(14)	118.2	118.2	118.5	117.8	117.8
C3—C4—C5	120.62(14)	121.1	121.0	121.3	121.3	121.5
C6—C7—C1	120.34(14)	119.2	119.1	119.3	118.7	118.6
C1—C7—N1	115.79(13)	117.1	117.2	116.1	117.4	118.4
N1—C8—C9	123.72(14)	123.2	123.0	121.9	121.7	124.9
C8—C9—C10	120.71(13)	119.9	120.0	118.8	120.9	122.7
O2—C10—C11	122.16(14)	122.6	122.6	122.7	118.8	121.3
C11—C10—C9	116.24(13)	115.7	116.0	115.5	119.2	115.5
C11—C12—C13	121.09(14)	122.3	122.2	122.1	121.2	121.3
C14—C13—C12	118.65(14)	118.9	119.0	118.8	118.9	117.6
C13—C14—C9	121.79(14)	121.0	120.8	121.1	121.2	122.9
N2—N3—C15	114.39(12)	115.0	115.1	113.9	115.1	122.1
C20—C15—N3	115.43(13)	124.7	124.8	124.6	124.7	121.7
C17—C16—C15	119.56(14)	120.4	120.4	120.5	120.3	119.9
C19—C18—C17	119.93(15)	119.8	119.8	119.9	119.9	119.4
C19—C20—C15	120.37(15)	119.8	119.7	120.1	119.7	119.3

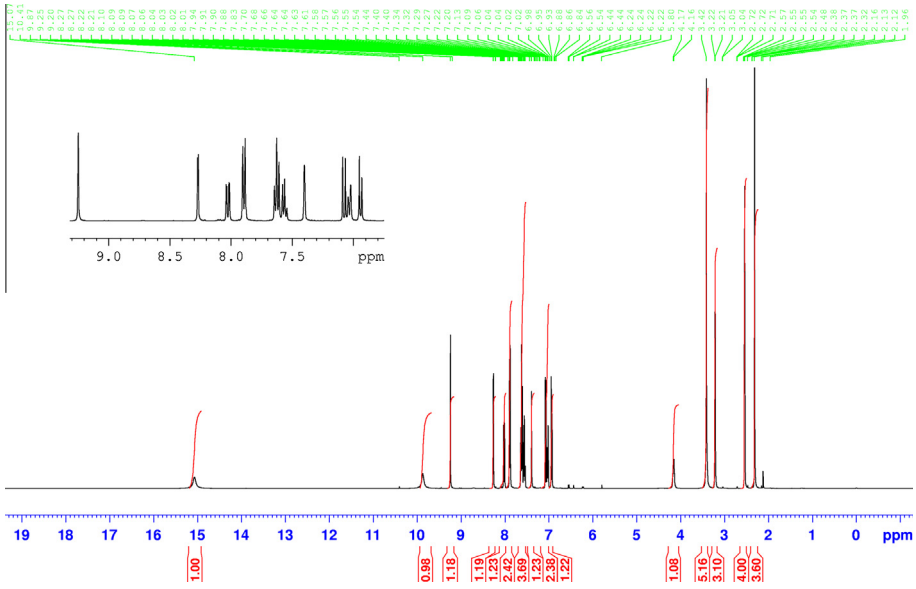

Fig. 1. ^{1}H NMR spectrum of the dye.

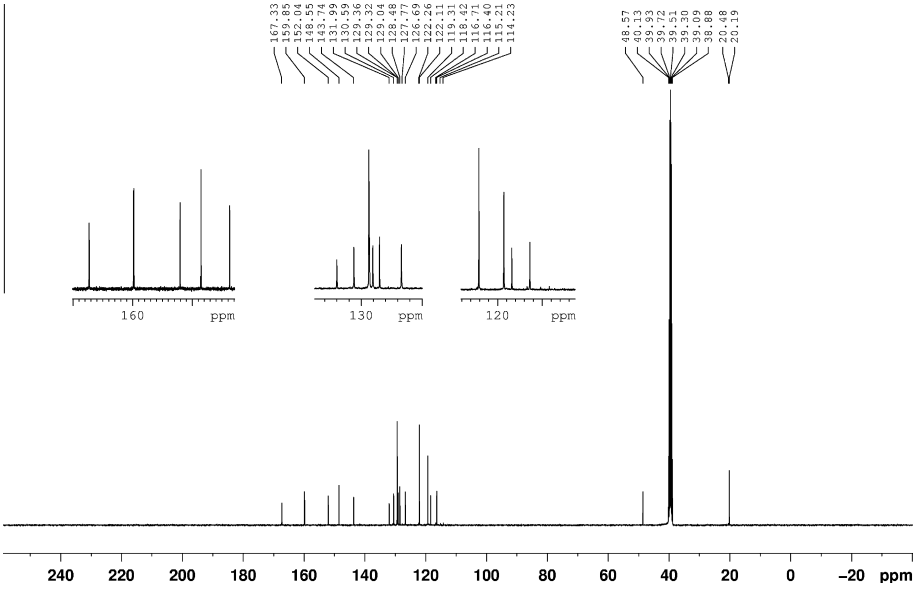

Fig. 2. ^{13}C NMR spectrum of the dye.

analysis results are given in the experimental section and are in good agreement with the calculated values. The data are in good agreement with single crystal X-ray determination.

3.2. Spectral characterization

3.2.1. NMR spectra

The ^{1}H NMR spectrum of the title dye displays a singlet at δ 2.16 ppm corresponding to protons of methyl group (Ph-CH_3). A singlet at δ 9.25 ppm was assigned to the proton of (—N—CH=) [33]. Two broad signals at δ 10.41 and 15.07 ppm could be assigned to protons of enamine (—NH—C=) and phenol (Ph-OH), respectively. The broad signal at the δ 4.17 ppm and the singlet at the δ 3.22 ppm the corresponding to methanol protons are indicative of presence of methanol solvate in the compound. Presence of methanol solvate in the compound was also confirmed by CHN analysis and single crystal X-ray diffraction study. All aromatic protons were observed in the range of δ 6.22–8.27 ppm.

The ^{13}C NMR spectrum of the compound exhibited the signals due to the presence of aromatic and methylene carbons. Two aliphatic carbon shifts were observed at δ 20.19 and 48.57 ppm assigned to methyl groups in aromatic ring and methanol molecule, respectively. The signal at δ 167.33 ppm could be assigned to the carbon (—NH—C=). All other aromatic carbon shifts were observed in the range of δ 114.23–159.85 ppm. ^{1}H and ^{13}C NMR spectra are displayed in Figs. 1 and 2, respectively. The NMR data showed that azo-enamine tautomer is maintained in DMSO and agreed with values reported in literature [33].

3.2.2. Mass spectrum

The ESI mass spectrum and mass fragmentation assignment of the compound is shown in Fig. 3 and Scheme 2. Mass spectrum of the dye showed signals at *m*/*z* 332 (26%) and 354 (100%)

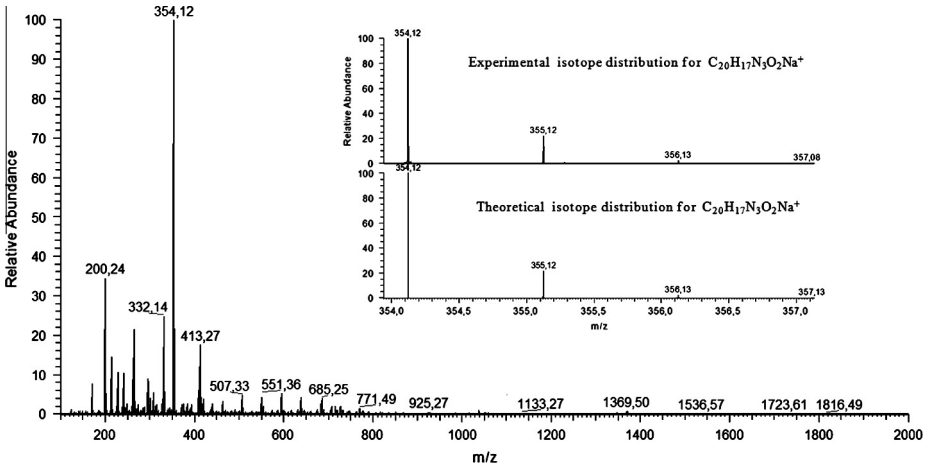

Fig. 3. ESI mass spectrum of the dye.

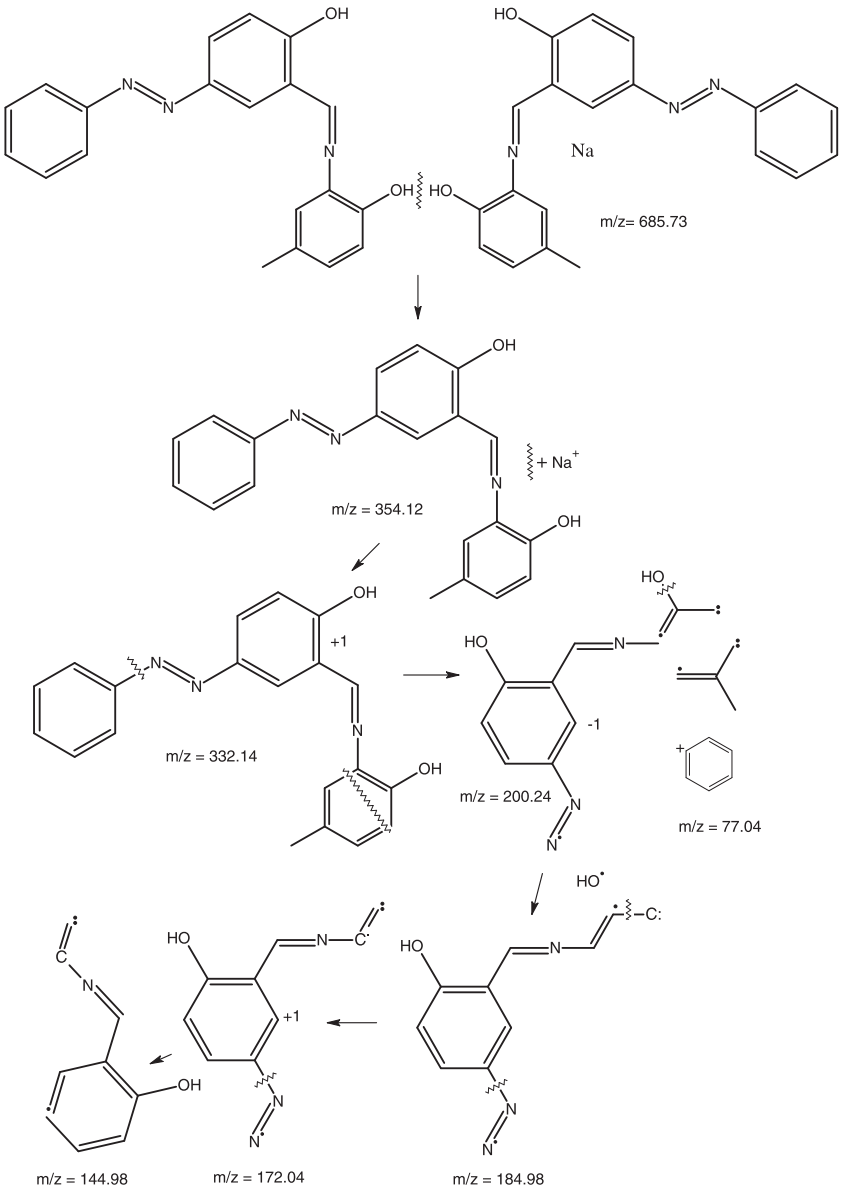

Scheme 2. Mass fragmentation pattern of the dye.

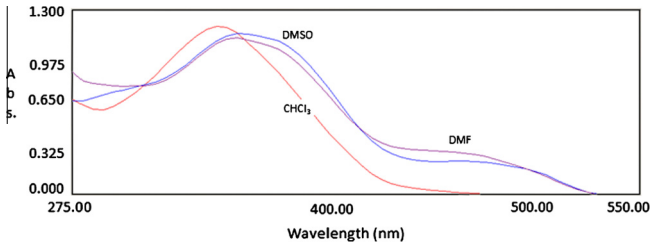

Fig. 4. Absorption spectra of the dye in different organic solvents.

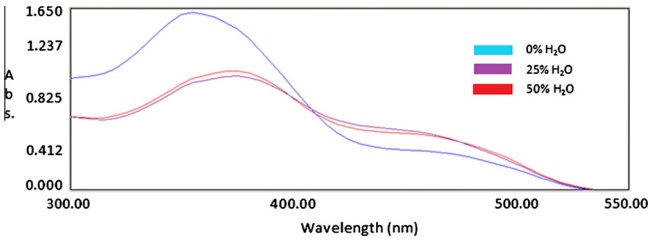

Fig. 6. Absorption spectra of the dye in DMF–H_2O mixtures.

assigned to $[M + H]^+$ and $[M + Na]^+$, respectively. The higher mass peak at *m*/*z* 685 (8%) was attributed to $[2M + Na]^+$. In the mass spectrum of the azo-azomethine compound, smaller fragmentations are also observed at *m*/*z* value of 200, 184, 172 and 142 and these fragmentations are assigned in Scheme 2.

3.2.3. IR spectrum

The IR spectrum of the dye shows several bands in 4000–450 cm^{-1} region. The bands of the dye are also listed in experimental section. The functional groups of the dye have been identified from the infrared spectrum. The band at 1614 cm^{-1} was assigned to C10═O2 and C7—N1 stretchings. Phenolic —OH group of the dye containing —N═N— chromophore group was characterized by an absorption band at 3370 cm^{-1}. The aromatic and aliphatic (methyl) moieties in the compound were identified by the bands at 3060 cm^{-1} (aromatic C—H stretching) and 2912 cm^{-1} (aliphatic C—H stretching). Two bands at 1480 and 1588 cm^{-1} were assigned to the azo group —N═N— and —C═C— (aromatic) stretchings, respectively. Bands at 1207 and 1141 cm^{-1} were assigned to the C—O and C—H (aromatic) stretchings, respectively. The synthesized dye may exist in three possible tautomeric forms, in solid state and solution namely (i) azo-imine form, (ii) azo-enamine form and (iii) hydrazone-imine form as depicted in Scheme 1. The single crystal X-ray diffraction study on the dye clearly indicates that the present compound exists in azo-enamine form rather than in azo-imine form and hydrazone-imine form in the solid state.

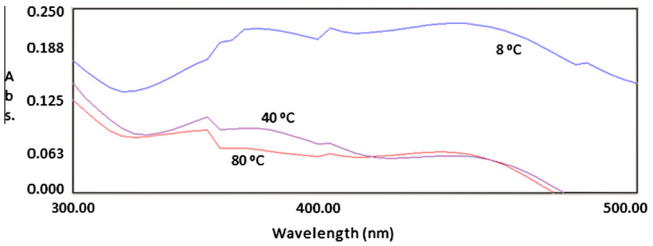

Fig. 7. Dependence of electronic absorption spectra of the dye on temperature in DMF.

3.2.4. Electronic absorption spectra

The UV–Vis absorption spectra of the synthesized dye were measured in the range of 275–550 nm in three organic solvents $CHCl_3$ DMSO and DMF ($C = 2.5 \times 10^{-5}$ M) at room temperature (Fig. 4). In $CHCl_3$, DMSO and DMF, maximum absorptions observed in the range of 345–355 nm were assigned to the $\pi \rightarrow \pi^*$ transitions of π electrons in the structure. Absorption intensity of the $\pi \rightarrow \pi^*$ transitions decreased in order of $CHCl_3$, DMSO and DMF (hyperchromic effect). The $\pi \rightarrow \pi^*$ transitions in chloroform which is an apolar and aprotic solvent was observed at shorter wavelength (hyposochromic effect) with higher absorption intensities (hyperchromic effect) than in DMF and DMSO. The $\pi \rightarrow \pi^*$ transitions in DMSO and DMF were observed approximately in the same

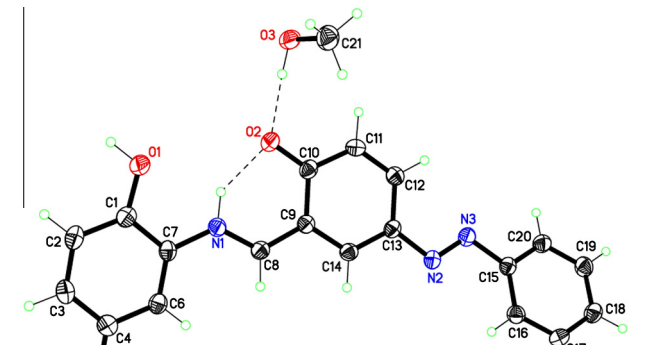

Fig. 8. Molecular structure with atom numbering thermal ellipsoid 50% probability.

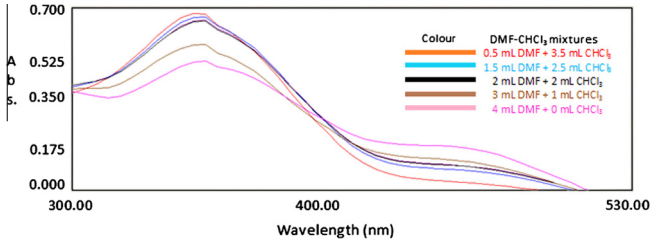

Fig. 5. Absorption spectra of the dye in DMF–$CHCl_3$.

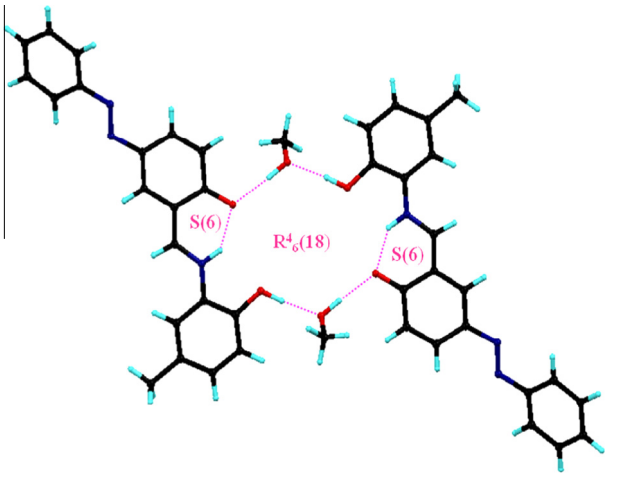

Fig. 9. Intra- and intermolecular hydrogen bonding within the structure. Symmetry code: $-x, -y, -z$.

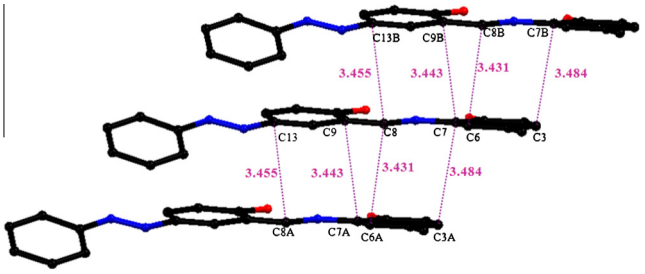

Fig. 10. π···π interactions within the structure of the dye.

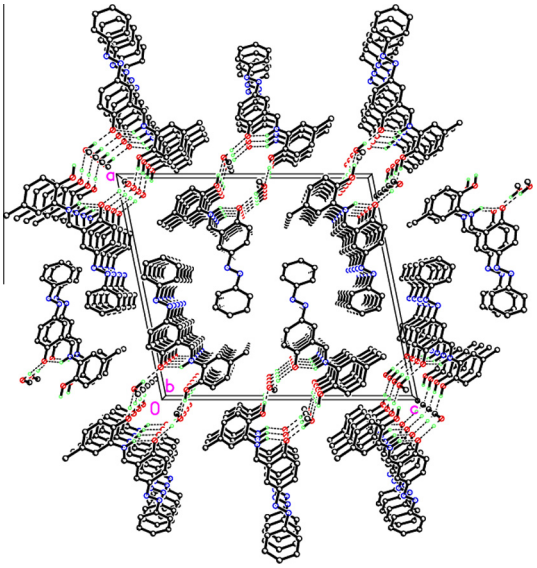

Fig. 11. Packing diagram, non-hydrogen bonded hydrogen atoms are omitted for clarity; hydrogen bonds are shown as dashed lines.

region with higher wavelength (batochromic effect). In both DMF and DMSO, an absorption band was observed in the 450–500 nm range assigned to the n → π* transitions of azo-aromatic chromophore and intermolecular charge transfer interaction [33,34]. The absorption intensity of n → π* transitions in DMF is higher than the same absorption intensity in DMSO. However, n → π* transitions were not seen in chloroform.

Table 5
Total and Gibbs free energies (kJ mol^{-1}) of tautomers **(1)**, **(2)** and **(3)**.

	Tautomer **(1)**	Tautomer **(2)**	Tautomer **(3)**
E (kJ mol^{-1})	−2853791.1	−2853805.9	−2853712.9
$G°$ (kJ mol^{-1})	−2853991.4	−2854003.2	−2853914.8

The UV–Vis absorption spectra of the dye at different volume ratios of the applied pair solvents DMF/$CHCl_3$ ($C = 2.5 \times 10^{-5}$ M) were also measured. The absorption curves of the dye in DMF–$CHCl_3$ mixtures are shown in Fig. 5. It can be seen from Fig. 5 that the absorption intensity at 350 nm decreased with increase in polarity of the solutions. However, the absorption intensity at 450–500 nm increased with increase in polarity of the mixtures.

The UV–Vis absorption spectra of the dye at different volume ratios of the applied pair solvents DMF/H_2O were also measured (Fig. 6). No particular differences were observed in UV–Vis absorption spectra of the dye in water–DMF (25% and 50% Water/DMF) solutions. The π → π* transitions shifted to lower absorption intensity (hypochromic effect). However, the n → π* transitions in the range of 450–500 nm shifted higher absorption values.

The UV–Vis spectra of the compound in DMF solvent were worked in the range of 300–530 nm at 8 °C, 40 °C and 80 °C, respectively (Fig. 7). Absorption intensities of the compound decreased with the increase in temperature (hypochromic effect).

3.3. X-ray structure

Perspective view of the compound is shown in Fig. 8. The compound crystallizes in monoclinic crystal system, $P2_1/c$ space group with unit cell parameters $a = 18.541(2)$, $b = 4.7091(5)$, $c = 20.586(2)$ Å, $\beta = 101.460(2)°$, $V = 1761.5(3)$ Å^3 and $Z = 4$ (final refinement value $R = 0.0427$).

All bond lengths and angles are within the normal ranges. X-ray investigation of the compound showed that azo-enamine tautomer is favoured in the solid state. The C10—O2 bond length of 1.2811(17) Å indicates a double bond character, whereas the C8—N1 bond length of 1.3077(19) Å is longer than a double bond (C=N) character and the C8—C9 bond length of 1.408(2) Å is longer than a double bond (C=C) character.

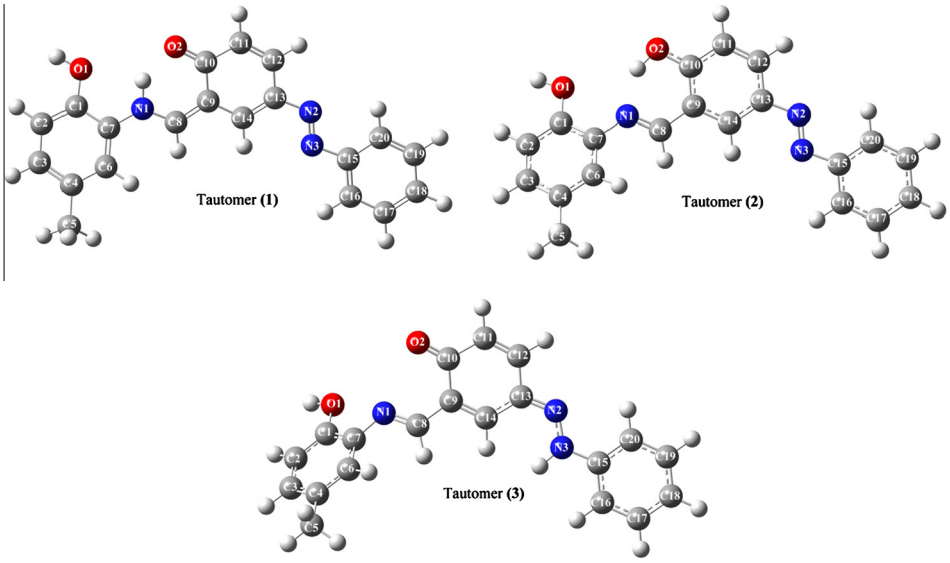

Fig. 12. Optimized structures of tautomers **(1)**, **(2)** and **(3)**.

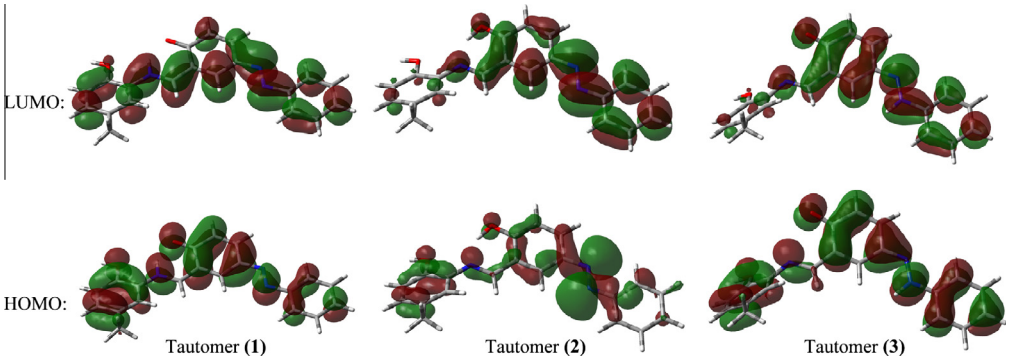

Fig. 13. Contour diagrams of frontier molecular orbitals for tautomers **(1)**, **(2)** and **(3)**.

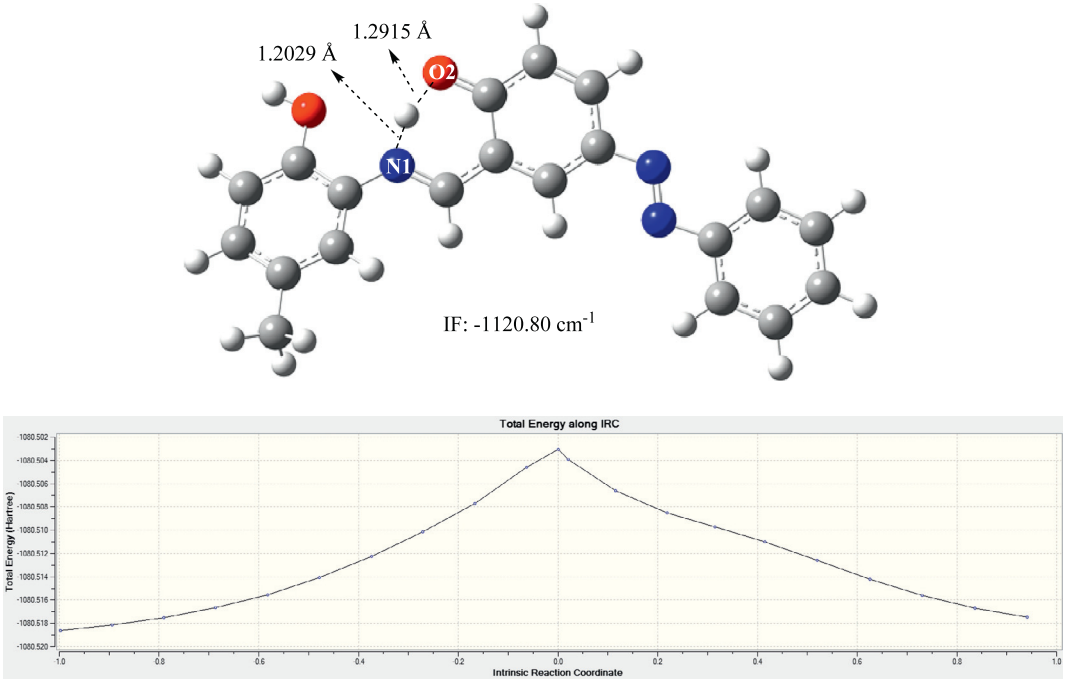

Fig. 14. The structure of transition state (upper) and IRC graphic (below).

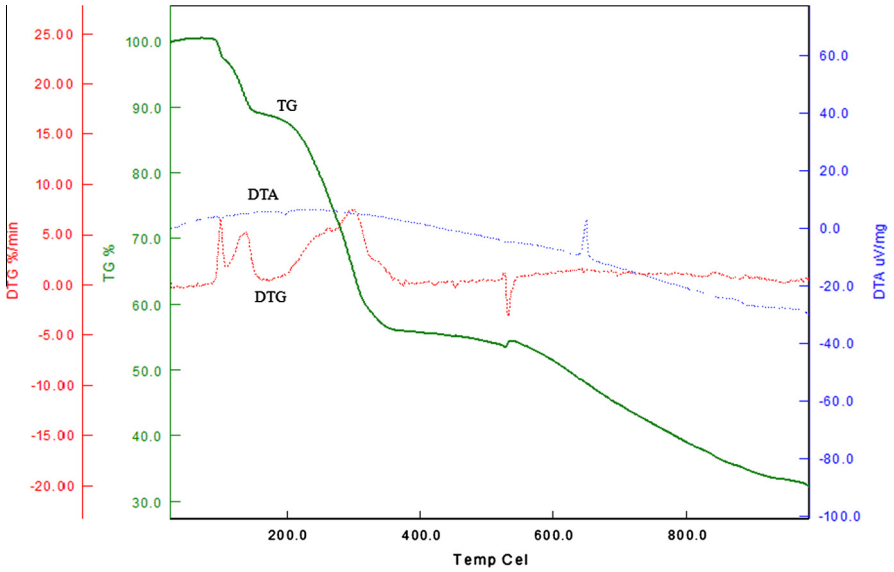

Fig. 15. TGA–DTA curves for the dye.

Table 6
Thermal analyses data for the dye.

Decomposition steps	DTA peak range (°C)	TG range (°C)	DTG_{max} (°C)	%Wt. loss Calcd. (Found)	Assignments
I	99 (endo)	68–104	98	(3.1)	Loss of H_2O lattice
II	–	104–172	135	(8.8)	Loss of CH_3OH lattice
III	197 (endo)	172–387	296	(33)	Loss of 4-methylphenol unit
IV	529 (endo)	387–605	532	(4.6)	
Residue	649 (exo)	–	–	(50.5)	

Aromatic rings (C9—C14) and (C15—C20) adopt the *trans* configuration with regard to the azo double bond (—N2═N3—) with a distance of 1.2617(17) Å the torsion angle C13—N2—N3—C15 of 174.54(12) Å which is in good agreement with published values [25].

The molecules crystallise as dimers, assembled by two methanol molecules *via* intermolecular hydrogen bonding. A methanol solvate involved in hydrogen bonding with both central (as donor) and outer phenol groups (as acceptor) linking two molecules together resulting in a $R_6^4(18)$ hydrogen bonding motif. There is also an intramolecular hydrogen bonding (N—H···O) in the molecule forming a S(6) graph set motif (Fig. 9) (Table 2).

In the structure, the azo benzene ring slightly twisted with respect to the central benzene ring. The mean planes of C1—C7 and C15—C20 are at 6.31(9) and 24.94(7)° to the central (C9—C14) ring, respectively. This is possibly a consequence of the intermolecular interactions in the lattice. Dimeric units in the structure are linked *via* π–π interactions, C6 and C8 is separated by a distance of 3.431 Å (under symmetry operation of $x, -1 + y, z$) (Fig. 10). Crystal packing of the compound is determined by intermolecular hydrogen bonding and π–π interactions. The packing plot of the compound is shown in Fig. 11.

3.4. Optimized structures

Fig. 12 shows the optimized structures of tautomers **(1)**, **(2)** and **(3)**. Calculated bond lengths and angles of tautomers **(1)**, **(2)** and **(3)** were given in Tables 3 and 4, respectively.

Compared with experimental and calculated bond lengths/angles of tautomer **(1)**, it can be seen that B3LYP/6-311G(d,p) level is the best level. The differences average between experimental and calculated bond lengths of tautomer **(1)** is 0.009 Å. The differences average between experimental and calculated bond angles of tautomer **(1)** is 1.6°. These results show that there is a good agreement between experimental and optimized structure of tautomer **(1)**.

3.5. The stability of tautomers

The total energy (E) and Gibbs free energy ($G°$) were calculated to predict the stability of tautomers in gas phase and given in Table 5.

The tautomer with the lowest energy has the most stability. The stability ranking of tautomers should be:

(2) > **(1)** > **(3)** (according to the E)
(2) > **(1)** > **(3)** (according to the $G°$)

Taken into account E and $G°$, the most unstable tautomer is tautomer **(3)**. However, E and $G°$ of tautomers **(1)** and **(2)** are close each other. For E and $G°$, the differences of energies are 14.8 and 11.8 kJ mol^{-1}, respectively. These differences indicates that tautomers **(1)** and **(2)** can be easily transformed each other. The determination of stability is difficult between tautomers **(1)** and **(2)**.

Table 7
Zone of inhibition for the dye against the selected microbes.

Concentration (%)	Zone of inhibition (diameter, mm)			
	Gram (−)		Gram (+)	
	E. coli	*K. pneumoniae*	*B. cereous*	*S. aureus*
1	–	–	26	22
2	–	–	28	24
3	–	–	28	28
4	–	–	30	29
DMSO(control)	–	–	–	–

–: ineffective.

Contour diagrams of HOMO and LUMO can be used to predict the reactive region of tautomers. Contour diagrams of frontier molecular orbitals of tautomers were represented in Fig. 13. HOMO and LUMO of tautomers are mainly delocalized on all atoms of molecules.

3.6. Transition state

The transformation between tautomer **(1)** and tautomer **(2)** was investigated by using transition state method. Because Gibbs free energy and total energy of tautomer **(1)** and **(2)** are close to each other. The transition state (TS) was calculated to explain the transformation. Imaginary frequencies (IF) indicate that the calculated structure is the transition state. The optimized structure of the transition state and intrinsic reaction coordinate (IRC) versus total energy graphic were represented in Fig. 14.

As can be seen from IRC graphic, the highest energy state corresponds to optimal transition state. The optimal transition state has −1120.80 cm^{-1} negative frequency. The distances between N1···H and O2···H were obtained as 1.2029 Å and 1.2905 Å, respectively. The structure of the TS are closer to the tautomer **(1)** than to the tautomer **(2)**. Because N1···H distance is smaller than O2···H distance [35]. This result indicates that tautomer **(1)** is more stable than tautomer **(2)** in the gas phase.

3.7. Thermal analyses

Thermal analysis of the dye was performed on SII Exstar TG/DTA 6200. Thermal stability of the dye (~1 mg) was studied in the temperature range of 30–1000 °C under nitrogen atmosphere at a heating rate of 20 °C/min. The thermal analysis curves (TG and DTA) of the studied complex are shown in Fig. 15. Thermal decomposition data for the compound is illustrated in Table 6. The examination of TG and DTA curves that the compound has four decomposition steps. It was found that the compound thermally stable up to 172 °C and started to lose mass in the 68–104 °C range (3%). In the second step, 8.8% of the compound was lost. These two decomposition steps (3.3% and 8.8%) correspond to loss of the hydrate water and methanol solvates in the structure, respectively. Thermal decomposition of the framework of the title dye starts at 172 °C. In the 172–387 °C range the mass loss was 33% and this was assigned to the loss of 4-methylphenol unit of the dye.

Further mass loss was observed in the 387–605 °C with a 4.6% mass loss.

3.8. Antimicrobial activity

The effect of the dye different concentrations on antimicrobial activity was studied further and the results are summarized in Table 7. A zone of inhibition (diameter, mm) was determined in each case. It was observed that an increase in concentration lead to an increased zone of inhibition as can be seen by the enhancement in the zone diameter. The compound shows antibacterial effect to gram positive *B. cereous* and *S. aureus* bacteria in different levels. However it is not effective on the gram negative *E. coli* and *K. pneumoniae* bacteria. It was observed that inhibition activity increased with increasing concentration of the synthesized the dye used. The efficacy of the dye dissolved in the dimetysulfoxide may be originated from the cell wall composition of the gram positive bacteria, or this substance may inhibit the enzyme systems of gram positive bacteria in a different manner than that of the gram negative bacteria [36].

4. Conclusion

In summary, the title dye, 2-{(*E*)-[(2-hydroxy-5-methylphenyl)imino]methyl}-4-[(*E*)-phenyldiazenyl]phenol, was prepared *via* a Schiff base condensation reaction and characterized by UV–Vis, IR, ^{1}H, ^{13}C NMR, mass spectrometry and elemental analyses. The molecular structure of the dye was successfully determined by single crystal X-ray diffraction study. The single crystal X-ray diffraction data clearly indicates that the present compound exists in azo-enamine form rather than azo-imine and hydrazone-imine form in the solid state. The molecules crystallize as dimers, assembled by two methanol molecules *via* intermolecular hydrogen bonding. The π–π interactions were observed in the structure. The title compound was found to be effective against gram positive bacteria and increase in concentration enhances the activity. The dye did not show any activity against gram negative bacteria.

Acknowledgements

The author thanks to Research Found of Kahramanmaras Sutcu Imam University for financial support (Project No: 2011/8-5 YLS), Kahramanmaras, Turkey and Department of Chemistry, Loughborough University for providing laboratory and analytical facilities. Theoretical calculations were made possible by TUBITAK ULAKBIM (TR-Grid e-Infrastructure).

References

[1] R. Gup, E. Giziroglu, B. Kırkan, Dyes Pigments 73 (2007) 40–46.
[2] H.E. Katz, K.D. Singer, J.E. Sohn, C.W. Dirk, L.A. King, H.M. Gordon, J. Am. Chem. Soc. 109 (21) (1987) 6561–6563.
[3] M. Gaber, T.A. Fayed, S. El-Daly, Y.S.Y. El-Sayed, Spectrochim. Acta Part A 68 (2007) 169–175.
[4] S.S. Kandil, Transit. Metal Chem. 23 (1998) 461–465.
[5] D.W. Rangnekar, V.R. Kanetkar, J.V. Malanker, G.S. Shankarling, Indian J. Fibre Text. Res. 24 (1999) 142–144.
[6] M. Kurtoglu, N. Birbicer, U. Kimyonsen, S. Serin, Dyes Pigments 41 (1999) 143–145.
[7] A.A. Jarrahpour, M. Motamedifar, K. Pakshir, N. Hadi, M. Zarei, Molecules 9 (10) (2004) 815–824.
[8] A.J. Blake, N.R. Champness, P. Hubberstey, W.S. Li, M.A. Withersby, M. Schroder, Coord. Chem. Rev. 183 (1999) 117–138.
[9] P.A. Vigato, S. Tamburini, Coord. Chem. Rev. 248 (2004) 1717–2128.
[10] A.Y. Robin, K.M. Fromm, Coord. Chem. Rev. 250 (2006) 2127–2157.
[11] S. Akine, T. Nabeshima, Dalton Trans. 47 (2009) 10395–10408.
[12] D.R.C. Matazo, R.A. Ando, A.C. Borin, P.S. Santos, J. Phys. Chem. A 112 (2008) 4437–4443.
[13] P.I. Nagy, W.M.F. Fabian, J. Phys. Chem. B 110 (2006) 25026–25032.
[14] H.Y. Lee, X. Song, H. Park, M.-H. Baik, D. Lee, J. Am. Chem. Soc. 132 (2010) 12133–12144.
[15] W.M.F. Fabian, L. Antonov, D. Nedeltcheva, F.S. Kamounah, P.J. Taylor, J. Phys. Chem. A 108 (2004) 7603–7612.
[16] A.G. Gilani, M. Moghadam, M.S. Zakerhamidi, E. Moradi, Dyes Pigments 92 (2012) 1320–1330.
[17] (a) H. Khanmohammadi, K. Rezaeian, Spectrochimica Acta Part A 97 (2012) 652–658;
(b) M. Odabaşoğlu, Ç. Albayrak, O. Büyükgüngör, P. Lonnecke, Acta Cryst. C59 (2003) o616;
(c) M. Odabaşoğlu, Ç. Albayrak, O. Büyükgüngör, H. Goesman, Acta Cryst. C59 (2003) o234.
[18] M. Kurtoglu, E. Ispir, N. Kurtoglu, S. Serin, Dyes Pigments 77 (2008) 75–80.
[19] M. Kurtoglu, S. Serin, Synth. React. Inorg. Met. Org. Chem. 31 (2001) 1129–1139.
[20] M. Kurtoglu, Synth. React. Inorg. Met. Org. Chem. 34 (2004) 967–977.
[21] M. Kurtoglu, S.A. Baydemir, J. Coord. Chem. 60 (2007) 655–665.
[22] H. Khanmohammadi, M. Darvishpour, Dyes Pigments 81 (2009) 167–173.
[23] Bruker, *APEX2* and *SAINT* Bruker *AXS* Inc, 1998.
[24] GaussView 5.0, (Gaussian Inc., Wallingford, CT, USA), 2009.
[25] Gaussian 09, AM64L-Revision-C.01, (Gaussian Inc., Wallingford, CT, USA), 2010.
[26] R.G. Parr, W. Yang, Density–Functional Theory of Atoms and Molecules, Oxford University Press, New York, 1989. p. 333.
[27] N. Niazazari, A.L. Zatikyan, S.A. Markarian, Spectrochim. Acta Part A 110 (2013) 217–225.
[28] D.A. Becke, J. Chem. Phys. 98 (1993) 5648–5652.
[29] C. Lee, W. Yang, R.G. Parr, Phys. Rev. B 37 (1988) 785–789.
[30] P.J. Hay, W.R. Wadt, J. Chem. Phys. 82 (1985) 270–283.
[31] J. Baker, J. Comp. Chem. 7 (1986) 385–389.
[32] G.M. Sheldrick, Acta Cryst. A64 (2008) 112–122.
[33] A. Kakanejadifard, F. Azarbani, A. Zabardasti, S. Kakanejadifard, M. Ghasemian, F.E. Ashari, S. Omidi, S. Shirali, M. Rafieefar, Dyes Pigments 97 (2013) 215–222.
[34] Z. Rezvani, A.R. Abbasi, K. Nejati, M. Seyedahmadian, Polyhedron 24 (2005) 1461–1470.
[35] N. Karakus, R. Ozkan, J. Mol. Struct.-THEOCHEM 724 (2005) 39–44.
[36] W.K. Jung, H.C. Koo, K.W. Kim, S. Shin, S.H. Kim, Y.H. Park, App. Environ. Micro. 74 (2008) 2171–2178.